Hindawi
Advances in Civil Engineering
Volume 2018, Article ID 6289721, 12 pages
https://doi.org/10.1155/2018/6289721

Research Article

Load Transfer Mechanism of Hybrid Pylon Joint with Cells and Bearing Plates

Yongjun Li,[1] **Yuqing Liu**,[2] **Feihua Wang**,[2] **and Fei Yang**[2]

[1]*Shanghai Municipal Engineering Design Institute (Group) Co., Ltd., Shanghai 200092, China*
[2]*Department of Bridge Engineering, Tongji University, Shanghai 200092, China*

Correspondence should be addressed to Fei Yang; 1510207@tongji.edu.cn

Received 1 August 2018; Accepted 4 December 2018; Published 24 December 2018

Academic Editor: Mario D'Aniello

To investigate the load transfer mechanism of the steel-concrete hybrid pylon joint with cells and bearing plates, a theoretical model based on the continuous elastic interlayer method was established. Both the slip effect at the steel-concrete interface and the local compression effect of the bearing plate were considered in the proposed theoretical model. A segment model test with a 1 : 3 scale was carried out to obtain the strain distribution of the hybrid joint and the relative slip between steel and concrete components. Finite element analysis was implemented on the tested segment model, and the structural performance of the tested hybrid joint was compared with the FEA results. The test and analysis results show that the stress of steel and concrete components is at a lower level, and the relative slip between steel and concrete components is extremely limited. The bearing plates and shear connectors are the two load-transferring components and could transfer 40% and 60% of the vertical force into the lower concrete pylon, respectively. The vertical force of shear connectors is at a much lower magnitude within 0.6 times the length of the hybrid joint from the bearing plate and will increase gradually within 0.6 to 1.0 times the length of the hybrid joint. The FEA results are in good agreement with the model test results, and the maximum shear force difference between the theoretical analysis results and the FEA results is less than 10%, proving that the proposed theoretical model can reasonably predict the shear force distribution at the steel-concrete interface of the hybrid joint. In addition, the stiffness of shear connectors has limited effect on the shear force distribution at the steel-concrete interface.

1. Introduction

Steel and concrete have been the two most practical and prevailing building materials in the construction of bridge infrastructures for many decades. Generally, there are four types of bridge components according to the arrangement of these two construction materials, including steel components, concrete components, steel-concrete composite components, and steel-concrete hybrid components. The composite component is an effective connection of the steel member and the concrete member in the cross-sectional level, while the hybrid component is a reasonable combination of the steel member and the concrete member along the longitudinal direction of the component [1–3]. Selecting or devising reasonable and suitable cross sections for each component of a bridge structure is the obligation and pursuit of bridge designers. In the pylon design of cable-stayed bridges, the designer is supposed to work out the most suitable structural configuration from the above four types of components to satisfy both the mechanical and the aesthetic requirements of the bridge pylon.

In recent years, the newly built cable-stayed bridges in China normally need to provide a much wider bridge deck to meet the growing traffic volume. The increasing operating traffic load and the much larger structural gravity of the bridge deck will be transferred in the bridge pylon through the cable-girder anchorage system, the cables, and the cable-pylon anchorage system. The huge cable force in these cable-stayed bridges requires an advanced cable-pylon anchorage system to ensure the load transfer reliability. If the concrete pylon scheme is selected, the steel-concrete composite cable-pylon anchorage structure could be adopted for the accelerated construction, while the configuration of the composite cable-pylon anchorage

structure will be complicated. The steel-concrete hybrid pylon could be an alternative for the construction of the cable-stayed bridges, since the lower part of the pylon could be constructed as a concrete structure and the upper part of the pylon could be fabricated as a steel structure. Besides, the upper steel pylon is also beneficial to the cable-pylon anchorage system and the accelerated bridge construction [4–6]. The combination of the upper steel pylon and the lower concrete pylon is the joint of the steel-concrete hybrid pylon, and its load transfer mechanism is the study objective of this paper.

Many studies have been conducted to investigate the performance of steel-concrete hybrid structures especially for hybrid girders. Kim and Nguyen [7, 8] developed a nonlinear finite element model to examine the behavior of the hybrid steel-PSC beam connection, and some efficient connection details were recommended. Kim et al. [9, 10] conducted three tests on small-scale steel-PSC hybrid beams to determine and to propose the suitable joint for spliced hybrid I-girder bridges. Besides, a full-scale test was conducted on a spliced steel-PSC hybrid I-girder of 40 m length to verify the new type of the joint splicing steel-PSC segment. In the steel-concrete joint of hybrid girders, perfobond rib (PBL) connectors have become another effective load transfer component owing to their superior mechanical performance, convenient construction, and extended service life. In recent years, a series of studies were implemented to examine the shear performance and load transfer mechanism of PBL connectors especially employed in the hybrid girder of cable-stayed bridges [11–17]. However, the existing studies mainly focus on the load-sharing distribution in the multiple PBL connectors, and the ratio of the load transferred by the bearing plate to the load transferred by the headed stud or PBL connectors was not investigated in detail. The configurations of the hybrid girder and the hybrid pylon in cable-stayed bridges have some common characteristics, such as the employment of headed studs and/or PBL connectors. The load transfer mechanism in the connecting part of the hybrid pylon is still worth to be investigated.

In this paper, a theoretical model for exploring the load transfer mechanism in the steel-concrete connecting part of the hybrid pylon is introduced firstly. Then, a scaled model of the connecting part, taken the hybrid pylon of Jishui Gan River Second Bridge as the prototype structure, was fabricated and tested. The load-sharing ratio by the bearing plate and the shear connector was measured, and the load transfer mechanism in the connecting part of the hybrid pylon was analyzed.

2. Prototype Bridge

Figure 1 shows the main-span structure of Gan River Second Bridge in Jishui County, Jiangxi Province, China. The main-span bridge is a cable-stayed bridge with two identical hybrid pylons, and the span arrangement is 2×110 m. The main girder of the bridge is a prestressed concrete girder, and the bridge pylon is a steel-concrete hybrid structure. The total width of the bridge deck is 38 m, while the transversally central distance between the two pylons is 28 m. Steel pylon was employed in the upper part of the bridge pylon for simplifying the configuration of the cable-pylon anchorage system and accelerating the construction of the bridge pylon. Concrete pylon was employed in the lower part of bridge pylon, since the configuration of the concrete pylon would be relatively simple compared with that of the steel pylon subjected to the huge compressive force. The upper part of the steel pylon was connected to the lower part of the concrete pylon through the connecting hybrid joint. The total height of the hybrid pylon is 90 m, and the heights of the lower-part concrete pylon and the upper-part steel pylon are 39.5 m and 45.8 m, respectively, while the height of the steel-concrete hybrid pylon joint is 4.7 m. Both PBL and headed stud connectors were employed below the bearing steel plate to transfer the vertical force from the upper concrete pylon.

Figure 1: Jishui Gan River Second Bridge.

Figure 2 shows the schematic view of the hybrid joint structure of Gan River Second Bridge. The steel-concrete hybrid joint is composed of the steel pylon stiffening transition part, steel-concrete connecting part, and concrete pylon transition part. All the pylon-cable anchorage zones are located at the steel pylon part, while the steel-concrete connecting part is just below the lowest cable-pylon anchorage position. The transition part of the steel pylon is stiffened with steel plates on the pylon wall plates and two vertical web plates. Two vertical web plates and the stiffeners run through the connecting part. Circular holes 75 mm in diameter were fabricated on the stiffening plates, and reinforcement bars 25 mm in diameter were set in each hole to form the perfobond rib (PBL) connectors. The headed studs 22 mm in diameter and 200 mm in height were welded on the interior steel plates, and the vertical spacing of the connecting part was 200 mm. In addition to the PBL and headed stud connectors, the bearing steel plate 60 mm in thickness was set on top of the concrete pylon to transfer the compression of the pylon.

3. Theoretical Analysis for the Connecting Joint

3.1. Basic Assumptions. The steel cells in the hybrid pylon joint are the basic component for transferring the vertical axial force from the upper steel pylon to the lower concrete pylon. As shown in Figure 3, in the steel cells of the hybrid connecting part, the vertical axial force of the steel pylon is mainly transferred to the concrete pylon through the compression action of the bearing plate and the shear connection action of the connector at the steel-concrete interface. The shear connectors include the headed studs welded on the pylon steel wall and steel web and the PBLs set

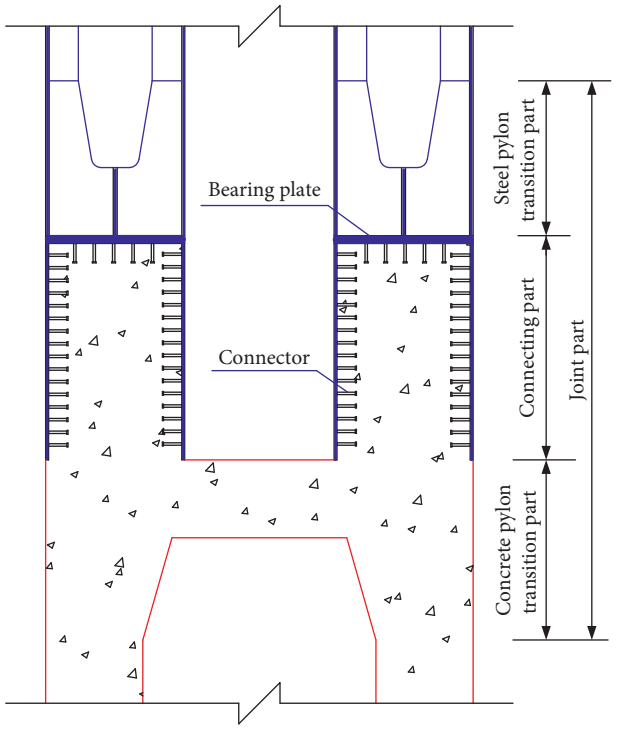

Figure 2: Schematic view of the hybrid joint structure.

on the steel stiffeners. Accordingly, a single steel cell with the rearing plate will be selected as the analyzing objective for studying the load transfer mechanism of the steel-concrete hybrid joint under compression. For obtaining the simplified load-transferring analyzing method, the following assumptions are introduced in the theoretical analysis:

(1) The strain of the pylon steel and concrete parts accords with the assumption of the plane section

(2) Small axial deformation is assumed and bending and shear deformation is ignored

(3) Both PBL and headed stud connectors are equivalent to the continuous spring layer

(4) The adhesive friction between the steel pylon wall and the concrete structure in the steel cells is neglected

3.2. Deformation Compatibility Equation and Static Equilibrium Equation. Figure 4 shows a simplified calculation model for the hybrid joint microbody. A segment dx is taken out from the simplified hybrid joint model as the microbody, and the vertical distance from the top of the joint to the position of the microbody is equal to x. $u_s(x)$ and $u_c(x)$ are the vertical displacements of the steel plate and the concrete wall in the microbody, respectively. $s(x)$ is the relative slip between the steel plate and the concrete wall. From the geometric relationship, the relative slip $s(x)$ could be expressed as

$$s(x) = u_s(x) - u_c(x). \tag{1}$$

In the microbody of the hybrid joint as shown in Figure 4, $N_s(x)$ and $N_c(x)$ represent the axial force of the steel plate and the concrete wall, respectively. Meanwhile, $q_\tau(x)$ stands for the shear force density at the steel-concrete interface, which was modelled as the spring layer. Then, the force balance conditions for the microbody should satisfy the following equations simultaneously:

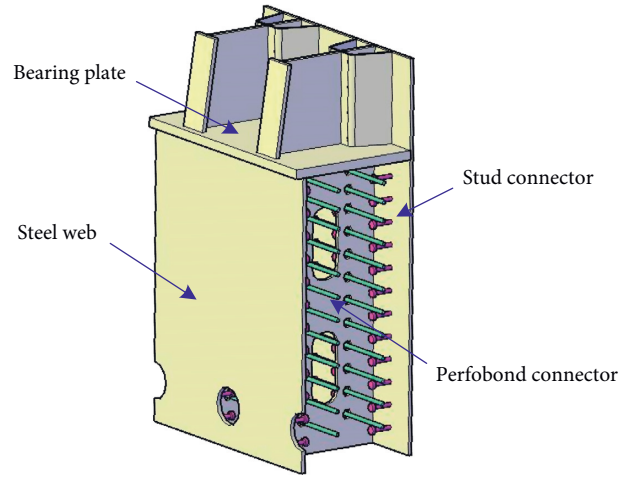

Figure 3: The structure detail of the steel cell in the hybrid joint.

$$q_\tau(x)\,dx = dN_s(x), \tag{2}$$

$$-q_\tau(x)\,dx = dN_c(x). \tag{3}$$

3.3. Physical Equation. It is assumed that both the steel plate and the concrete wall need to satisfy the Hooke law under the axial compression. The relationship between the axial force and the relative slip for these two elements in the microbody could be expressed as

$$\frac{N_s(x)}{E_s A_s} = \frac{du_s(x)}{dx}, \qquad \frac{N_c(x)}{E_c A_c} = \frac{du_c(x)}{dx}, \tag{4}$$

where E_s and E_c represent the elastic modulus of the steel plate and the concrete wall, respectively, and A_s and A_c stand for the cross-sectional area of the steel plate and the concrete wall, respectively.

For the shear connector at the steel-concrete interface, it is assumed that the shear force transferred by the shear connector including PBLs and headed studs is proportional to the relative slip at the steel-concrete interface; that is, all the shear connectors are in the linearly elastic state in the analysis. The constitutive model of the shear connector is shown in the following equation, which presents the relationship between the relative slip $s(x)$ and the shear force density $q_\tau(x)$:

$$q_\tau(x) = k_s s(x), \tag{5}$$

where k_s stands for the equivalent shear stiffness of the shear connector at the steel-concrete interface, which could be estimated based on the following equation:

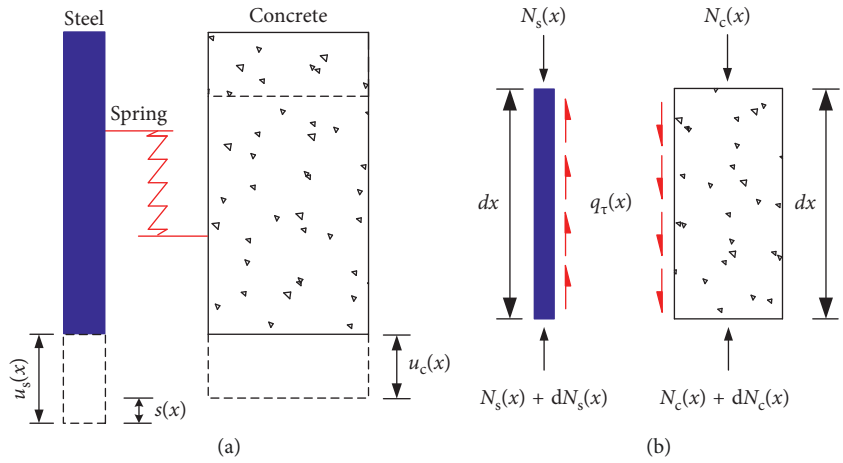

Figure 4: Relative slip and load distribution of the microbody. (a) Relative slip model. (b) Microbody.

$$k_s = \frac{n_{ss}k_{ss} + n_{sp}k_{sp}}{d}, \tag{6}$$

where n_{ss} and n_{sp} refer to the number of headed studs and perfobond plate connectors in the cross section, respectively; k_{ss} and k_{sp} mean the shear stiffness of headed studs and perfobond plate connectors, respectively; and d represents the vertical spacing of the shear connector.

3.4. Relative Slip Solution. To obtain the displacement and the shear force distribution at the steel-concrete interface, the relative slip at the steel-concrete interface is taken as the elementary unknown. Firstly, the second-order derivation is conducted on equations (1) and (6) which could be obtained as follows:

$$s''(x) = u_s''(x) - u_c''(x). \tag{7}$$

The second-order derivation of $u_s(x)$ and $u_c(x)$ could be obtained based on equation (4), respectively, and is exhibited in the following equations:

$$\begin{aligned} u_s''(x) &= \frac{N_s'(x)}{E_sA_s}, \\ u_c''(x) &= \frac{N_c'(x)}{E_cA_c}. \end{aligned} \tag{8}$$

Then, equations (2) and (3) are substituted into (8), respectively, and the second-order derivation of $u_s(x)$ and $u_c(x)$ in equation (7) could be replaced by the simplified equation (8). Accordingly, the following equation could be obtained:

$$s''(x) = \left(\frac{1}{E_sA_s} + \frac{1}{E_cA_c}\right)q_\tau(x). \tag{9}$$

Afterwards, the shear force density $q_\tau(x)$ in equation (9) can be replaced by equation (5), producing a differential equation relating with the relative slip at the steel-concrete interface as shown in the following equation:

$$s''(x) - \alpha^2 s(x) = 0, \tag{10}$$

where the introducing parameter α is equal to sqrt((1/E_sA_s+1/E_cA_c)k_s).

Equation (10) is a second-order homogeneous differential equation, and the general solution for this equation is shown as follows:

$$s(x) = C_1e^{\alpha x} + C_2e^{-\alpha x}, \tag{11}$$

where C_1 and C_2 are two undetermined coefficients, which can be determined by the boundary condition of the hybrid joint.

3.5. Boundary Condition. Figure 5 exhibits the schematic mechanical model of the steel cell structure in the connecting part of the hybrid pylon. The top bearing plate and the shear connector transfer the axial load into the concrete structures. At the interface between the top bearing plate and the concrete structure in the steel cell, i.e., $x = 0$ in the coordinate system of the mechanical model, the total axial force P applied on top of the bearing plate can be decomposed into two parts, which are the axial force P_s resisted by the steel plate and P_c transferred to the top surface of the concrete structure in the steel cell. At the end of the steel plate in the connecting part of the hybrid pylon, i.e., $x = L$ in the coordinate system of the mechanical model, the total axial force P will be transferred to the concrete structure completely.

It needs to be noticed that, at the interface between the bearing plate and the concrete structure, the concrete below the bearing plate is compressed unevenly, and the compressive stress of the concrete near the steel wall plate will be much larger. For simplifying the mechanical model of the concrete below the bearing plate, it is assumed that the concrete is only partially compressed at the edge of the steel wall plate. A vertical displacement still occurs in this part concrete under the axial load P_c. Therefore, the supporting effect on the bearing plate by the local concrete near the steel wall plate needs to be considered. In this paper, this supporting effect is regarded as an elastic spring, and the axial stiffness D_n of the elastic spring can be predicted as shown in the following equation:

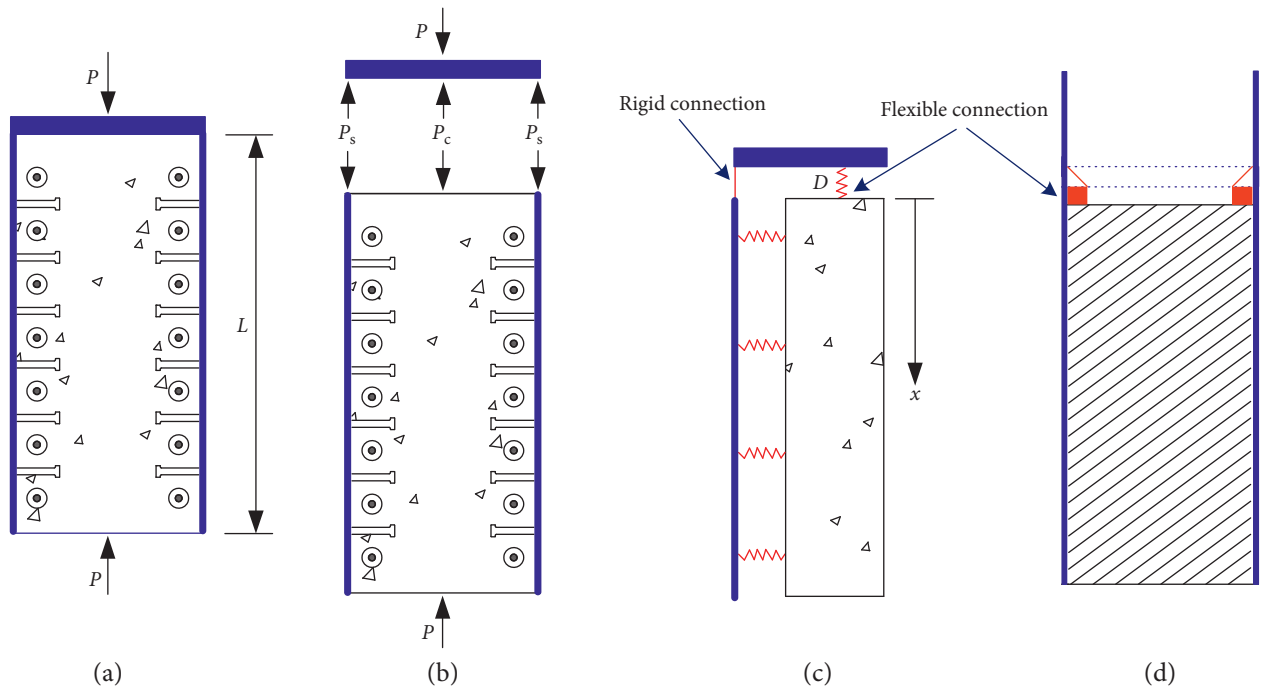

FIGURE 5: Theoretical analysis model for the joint. (a) Simplified model. (b) Force boundary condition. (c) Displacement condition. (d) Local compressive stress.

$$D_n = \frac{E_c A_z}{t_s}, \tag{12}$$

where t_s is the thickness of the bearing plate and A_z is the area of the partially confined concrete, which could be obtained through diffusing by 45° from the corner of the upper steel wall and the bearing plate to the top steel-concrete interface as shown in Figure 5(d); that is, the width of partially confined concrete equals the thickness of the bearing plate, and the length of the partially confined concrete equals that of the upper steel plate wall.

According to the above analysis, the displacement boundary conditions at $x = 0$ position will be as follows:

$$\begin{aligned} u_s'(0) &= \frac{P - P_c}{E_s A_s}, \\ u_c'(0) &= \frac{P_c}{E_c A_c}, \\ u_s(0) &= 0, \\ u_c(0) &= \frac{P_c}{D_n}. \end{aligned} \tag{13}$$

The displacement boundary conditions at $x = L$ position will be as follows:

$$\begin{aligned} u_s'(L) &= 0, \\ u_c'(L) &= \frac{P}{E_c A_c}. \end{aligned} \tag{14}$$

And then, the following equations could be obtained:

$$\begin{aligned} u_s'(0) - u_c'(0) &= \frac{P - P_c}{E_s A_s} - \frac{P_c}{E_c A_c} = s'(0), \\ u_s'(L) - u_c'(L) &= 0 - \frac{P}{E_c A_c} = s'(L), \\ u_s(0) - u_c(0) &= 0 - \frac{P_c}{D_n} = s(0). \end{aligned} \tag{15}$$

By substituting equation (11) and the deviation of equation (12) into equation (15), the two unknowns C_1 and C_2 could be obtained:

$$\begin{aligned} C_1 &= \frac{(P/\alpha E_c A_c) + e^{\alpha L}(\alpha + \beta)}{\alpha - \beta - e^{2\alpha L}(\alpha + \beta)}, \\ C_2 &= \frac{(P/E_s A_s)e^{2\alpha L} + (P/\alpha E_c A_c)e^{\alpha L}(\alpha - \beta)}{\alpha - \beta - e^{2\alpha L}(\alpha + \beta)}, \end{aligned} \tag{16}$$

in which the parameter β is shown as follows:

$$\beta = \frac{D_n}{E_c A_c} + \frac{D_n}{E_s A_s}. \tag{17}$$

3.6. Shear Force of Connectors. The total shear force of connectors at $x = x_i$ is the integral of the shear force of the continuous spring layer in the range of $(x_i - d/2, x_i + d/2)$, which can be obtained from equations (5) and (11) as follows:

$$V_s(x_i) = \int_{x_i - d/2}^{x_i + d/2} q_\tau(x)\,dx = \frac{k_s}{\alpha}\left(e^{\alpha \cdot d/2} - e^{-\alpha \cdot d/2}\right)\left(C_1 e^{\alpha x_i} + C_2 e^{-\alpha x_i}\right). \tag{18}$$

The shear force $V_{ss}(x_i)$ for headed studs and the shear force $V_{sp}(x_i)$ for PBLs at $x = x_i$ could be obtained according to their shear stiffness, as follows:

$$\begin{aligned} V_{ss}(x_i) &= \frac{1}{n_{ss}} \frac{n_{ss}k_{ss}}{n_{ss}k_{ss} + n_{sp}k_{sp}} V_s(x_i) \\ &= \frac{k_{ss}}{\alpha d}\left(e^{\alpha \cdot d/2} - e^{-\alpha \cdot d/2}\right)\left(C_1 e^{\alpha x_i} + C_2 e^{-\alpha x_i}\right), \\ V_{sp}(x_i) &= \frac{1}{n_{sp}} \frac{n_{sp}k_{sp}}{n_{ss}k_{ss} + n_{sp}k_{sp}} V_s(x_i) \\ &= \frac{k_{sp}}{\alpha d}\left(e^{\alpha \cdot d/2} - e^{-\alpha \cdot d/2}\right)\left(C_1 e^{\alpha x_i} + C_2 e^{-\alpha x_i}\right). \end{aligned} \tag{19}$$

4. Model Test for the Hybrid Joint

4.1. Test Model Configuration. Figure 6 shows the configuration of the test model for the hybrid joint, and a 1 : 3 scale test specimen was fabricated based on the configuration of the hybrid joint of Jishui Gan River Bridge. The height of the test specimen is 1936 mm in total, and the outline dimension of the steel wall plate is 1166 × 1268 mm. The concrete base was poured at the bottom of the test specimen as a supporting platform 300 mm in height, and its cross section outline dimension is 1766 × 1728 mm. A steel plate 20 mm in thickness was welded on top of the test specimen as the loading surface. In the test specimen, the perfobond plate and the headed stud connectors were arranged at the steel-concrete interface. The number of these shear connectors in the test specimen is the same as in the hybrid joint of the actual bridge. The hole diameter of the perfobond plate connector is 37.5 mm, and the steel bar 13 mm in diameter was employed to run through the hole. The headed studs are 13 mm in diameter and 80 mm in height, and the vertical spacing among the PBLs and the headed studs is 100 mm. Before the loading on the joint specimen, the mechanical properties of the steel plate and the concrete were measured, and Tables 1 and 2 show the average tensile properties for each steel plate employed in the joint specimen and the average mechanical properties for the poured concrete.

4.2. Test Loading Scheme. The loading test setup is shown in Figure 7. According to the finite element analysis for the actual bridge, the most unfavorable axial force in the hybrid joint of the single pylon is estimated to be 57200 kN. As the shear force and the bending moment at the hybrid joint are much smaller than the axial compressive force, the shear force and the bending moment were neglected and only the axial compressive force was loaded on the test specimen. According to the similarity criterion between the test specimen and the actual hybrid joint, the loading axial force P is set to be 6500 kN and the loading grade is 0.1P.

4.3. Measuring Program. The measuring point layout for the test specimen is shown in Figure 8. The strain gauges were used to monitor the strain of the steel plate in the test process. The measuring points on the external wall plate were A1, A2, A3, A4, A5, and A6 in a clockwise order, the measuring points on the longitudinal web were B1, B2, and B3, and the measuring points on the transverse web were C1, C2, C3, and C4. Seven rows of the measuring points were arranged from top to bottom of the specimen in total, and the numbering order is 1 to 7 from top to bottom of the specimen.

The embedded strain gauges were set in the steel lattice cells to measure the compressive strain of the concrete. The strain gauge numbers were F1, F2, F3, F4, and F5 in sequence as shown in Figure 8. There were 4 rows of strain-measuring points arranged from top to bottom corresponding to 1, 2, 3, and 4. The relative slip and the overall compressive displacement at the steel-concrete interface were measured using dial gauges. The relative slip gauge numbers were K1, L1, M1, and N1 and were set at the bottom of the joint. The dial gauge numbers that measured the overall compressive displacement are K2, L2, M2, and N2 and were placed on the bearing plate at the outside of the steel plate wall.

4.4. Test Results and Analysis. Figure 9 shows the load-slip curve between the steel plate and the concrete at the end of the joint. The relative slip at the three points under 1.0P axial force is 0.056 mm, 0.039 mm, and 0.039 mm, demonstrating that the relative slip at the steel-concrete interface is rather small. It can be concluded that the vertical deformation of the steel structure and the concrete structure accords with each other, and the hybrid joint has sufficient shear stiffness for transferring the axial load from the steel structure to the concrete structure.

Figure 10 shows the axial compressive stress distribution of the steel wall plate along the vertical direction of the hybrid joint at the measuring point of the steel structure under 1.0P axial load. With the increase of the distance from the bearing plate, the compressive stress of the steel plate tends to decrease gradually along the vertical direction of the test specimen, and the compressive stress of the steel plate diminishes rapidly in the position of the bearing plate, indicating that the bearing plate bears a large part of the axial load.

Figure 11 shows the compressive stress distribution of the interior concrete structure along the vertical hybrid direction at the measured point of the concrete structure under the 1.0P axial load. With the increase of the distance from the bearing plate, the compressive stress of the interior concrete tends to increase gradually along the vertical direction of the test specimen. On the contrary, the interior concrete will still be in the limited

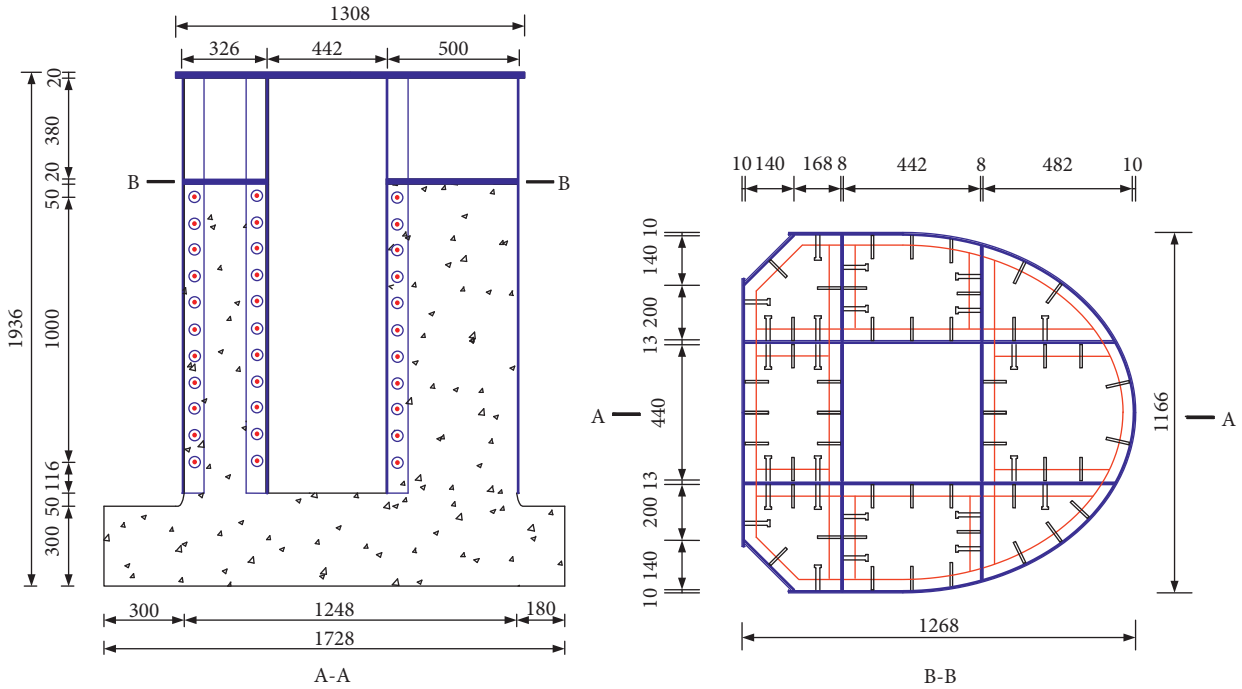

Figure 6: Details of the test specimen (unit: mm).

Table 1: Mechanical properties of the steel component.

Specimen	Plate thickness t (mm)	Yield strength f_y (MPa)	Tensile strength f_t (MPa)	Modulus of elasticity E_c (GPa)
Longitudinal steel web	13	347	466	213
Outer wall plate	10	350	471	211
Stiffened steel plate	8	377	512	196
Steel bar	—	480	548	199

Table 2: Mechanical properties of the concrete component.

Compressive strength f_{cu} (MPa)	Tensile strength f_t (MPa)	Modulus of elasticity E_c (GPa)
67.8	3.2	41.5

compressive state at the design axial load. From the bearing plate to the bottom of the hybrid joint, the axial force will be gradually transferred from the steel structure to the concrete structure.

Figure 12 shows the axial load of the steel structure and concrete structure along the vertical direction of the hybrid joint; the axial force could be estimated by the average stress in each region multiplied by the area of each region, and the average stress in each region equals the measured strain multiplied by the modulus of elasticity. It could be concluded from Figure 12 that the axial force taken by the concrete structure would gradually increase from top to bottom along the vertical direction of the test specimen, while the axial force taken by the steel plate gradually decreases from top to bottom along the vertical direction of the test specimen, proving that the force on the steel plate was gradually transferred to the concrete structure. The bearing plate was located between the first and second row measuring points of the steel plate. The difference between the axial force of the steel structure at these two rows of measuring points would be the axial force transferred by the bearing plate, i.e., 2540 kN. The top bearing plate could share approximately 40% of the axial load, and the remaining 60% of the axial load will be transferred from the steel structure to the concrete structure by the shear connector.

5. Finite Element Analysis and Comparison

5.1. Finite Element Model. The finite element model of the joint part was established using the finite element software ANSYS. Steel plates were modelled using the shell element SHELL63, and concrete components were modelled using the solid element SOLID65. The contact pressure at the steel-concrete interface was simulated by the contact element, while the adhesive friction between the contact surfaces was ignored. The shear connectors at the steel-concrete interface were modelled by a linear spring element, and the shear stiffness of the perfobond plate connector k_{ps} is shown by the following equation according to the Chinese specification JTG/T D64-1 [18]:

$$k_{ps} = 23.4\sqrt{(d - d_s)d_s E_c f_{ck}}, \tag{20}$$

where d is the diameter of the hole in the perfobond plate, d_s is the diameter of the reinforcement, E_c is the modulus of

Figure 7: Loading test setup.

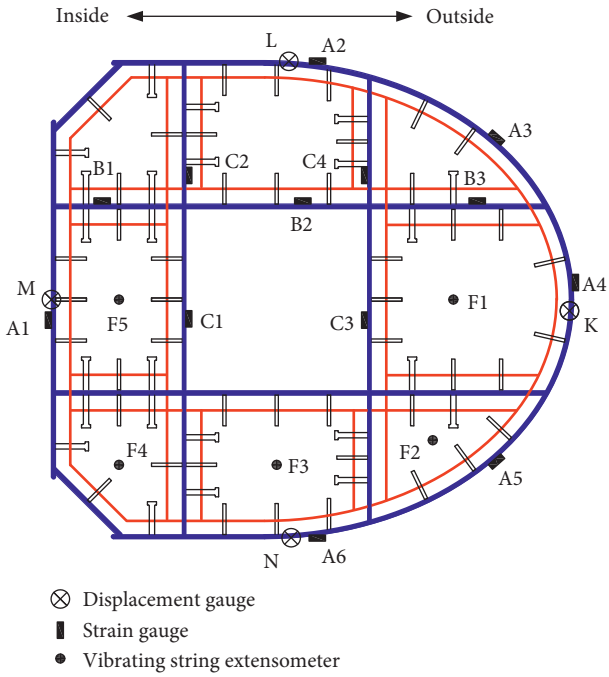

Figure 8: Layout of measuring positions.

elasticity of the concrete, and f_{ck} is the characteristic compressive cylinder strength of concrete.

The shear stiffness of the headed stud connector k_{ss} is shown by the following equation according to the study by Lin et al. [19, 20]:

$$k_{ss} = 0.32 d_s E_s^{0.25} E_c^{0.75}, \quad (21)$$

where d_s is the diameter of the headed stud and E_s is the modulus of elasticity of the steel.

5.2. Comparison of Finite Element and Test Results. Figure 13 shows the comparison results of the load-relative slip curves at the steel-concrete interface and the stress distributions in the steel plate and the internal concrete between the finite element analysis and the model test. It could be seen that the numerical analysis results including the relative slip and the stress distribution are in good agreement with the corresponding test results. The shear

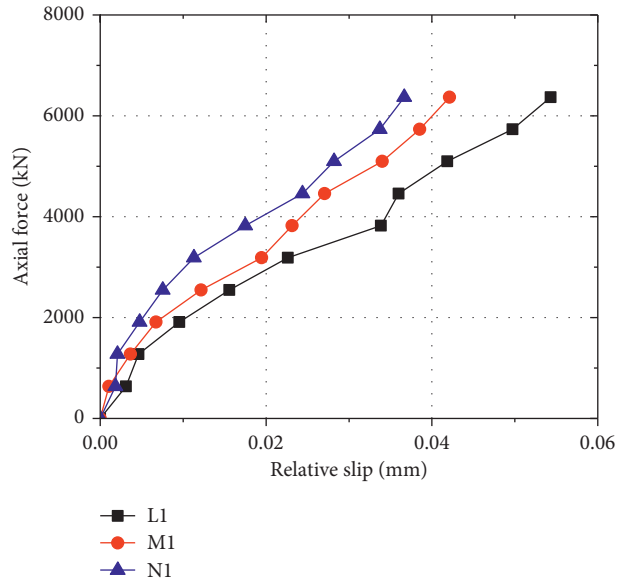

Figure 9: Load-slip curve of the test specimen.

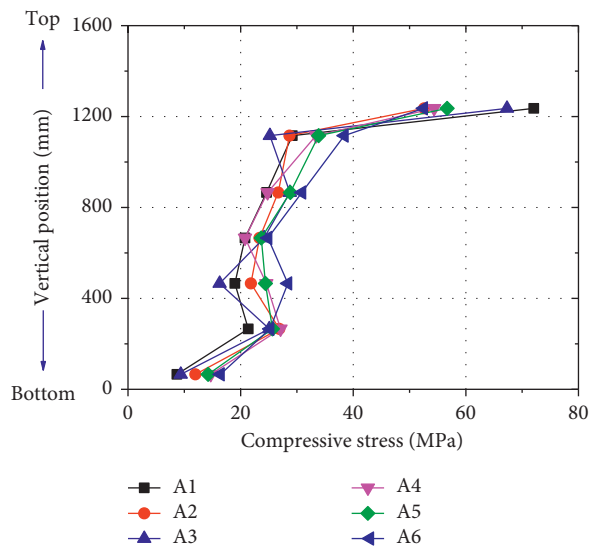

Figure 10: Stress distribution of the steel structure.

stiffness of the PBL and headed stud connectors based on equations (20) and (21) could provide enough accuracy for the simulation of the shear connector at the steel-concrete interface.

5.3. Comparison between Finite Element and Theoretical Results. Substituting the calculated parameters into equation (19), the average shear force of the connectors at each layer could be obtained. Other theoretical prediction results such as the axial compressive force supported by the steel plate and the concrete could also be obtained. Figure 14 shows the shear force comparison result of each layer shear connector between the finite element analysis and the theoretical analysis based on equation (19). It can be seen that the shear force results predicted based on the

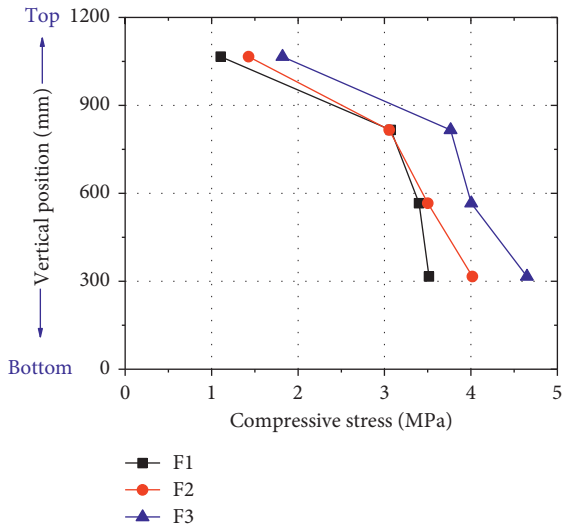

Figure 11: Stress distribution of the concrete structure.

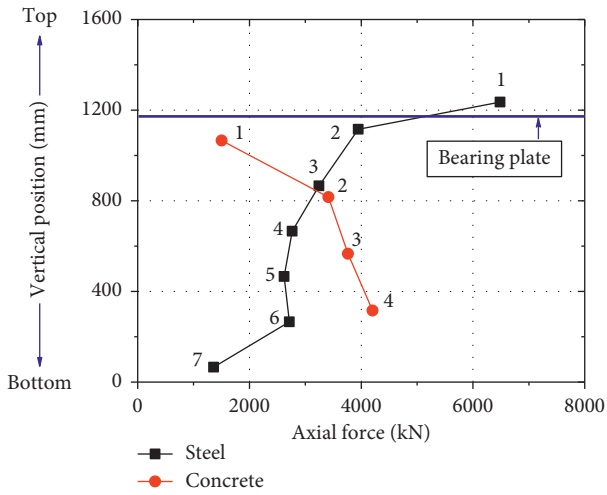

Figure 12: Distribution of axial force along the vertical direction shared by the steel and concrete structures.

theoretical analysis are almost identical to the results of the finite element analysis, and the maximum shear force of the shear connectors appears at the bottom position of the hybrid joint specimen, which is far away from the bearing plate. The maximum shear force of the connector by the theoretical analysis is 87 kN, and the difference between the theoretical analysis and the finite element analysis is less than 5%.

6. Theoretical Parameter Analysis for the Hybrid Joint

6.1. Steel-Concrete Relative Slip. The theoretical analysis method proposed in this paper is adopted to implement a parameter analysis based on the hybrid joint structure of the Jishui Gan River Second Bridge; meanwhile, the load transfer mechanism of the hybrid joint is discussed to provide a useful reference for the similar hybrid joint design.

Figure 15 shows the effect of the shear stiffness variation of the headed stud and perfobond plate connectors on the relative slip of the steel-concrete joint. In Figure 15, the zero position represents the interface between the top bearing plate and the concrete, and the downward direction along the hybrid joint is the positive direction. It could be seen from Figure 15 that the shear stiffness of the connectors has some obvious effect on the relative slip at the steel-concrete interface. With the increase of the distance from the top bearing plate to the bottom of the hybrid joint, the relative slip will decrease firstly and then increase till the bottom of the hybrid joint. The shear stiffness of the connectors may produce some influence on the decreasing and increasing trends of the relative slip. When the shear stiffness of the headed stud and perfobond plate connectors is reduced by 50%, the maximum value of the relative slip will increase from 0.076 mm to 0.118 mm with an increase of 55%. When the shear stiffness of the headed stud and perfobond plate connectors is doubly increased, the maximum relative slip will decrease from 0.076 mm to 0.047 mm with a decrease of 38%.

6.2. Joint Length Effect Analysis. Figure 16 shows the shear force distribution of the connectors at the steel-concrete interface with various joint length L. The joint length L is set to be $0.4B$ to $1.0B$, and B is the maximum width (equal to 3.5 m) of the joint along the longitudinal bridge in the single limb of the hybrid pylon. In each theoretical analysis model, the spacing of the headed stud and PBL connectors remains constant. When the joint length L is equal to half of the joint width ($0.6B$), the shear force of the connector will almost linearly increase from the top bearing plate to the bottom of the joint, and the shear force increases from 30 kN to 69 kN. When the joint length L continuously increases, more shear connectors are involved in transferring the shear force at the interface, while the shear force of the connectors near the bottom of the joint presents a gradual decreasing tendency. When the ratio of the joint length L to the joint width B exceeds 0.8, the variation of the shear force for the connectors near the top and bottom of the joint will be relatively small. The maximum magnitude of the connector shows an increasing tendency firstly and then a slightly decreasing tendency with the increase of the hybrid joint length, as shown by the dotted line in Figure 16.

6.3. Joint Axial Stiffness Effects. Figure 17 shows the relationship between the maximum shear force of the connector and the axial stiffness of the steel plate and the concrete component. E_sA_s and E_cA_c represent the axial tensile/compressive stiffness of the steel plate and the concrete component, respectively. It can be seen from Figure 17 that the maximum shear force of the connector at the steel-concrete interface has an increasing tendency with the increase of the axial tensile/compressive stiffness of the steel plate, while the maximum shear force of the connectors has a decreasing tendency with the increase of the

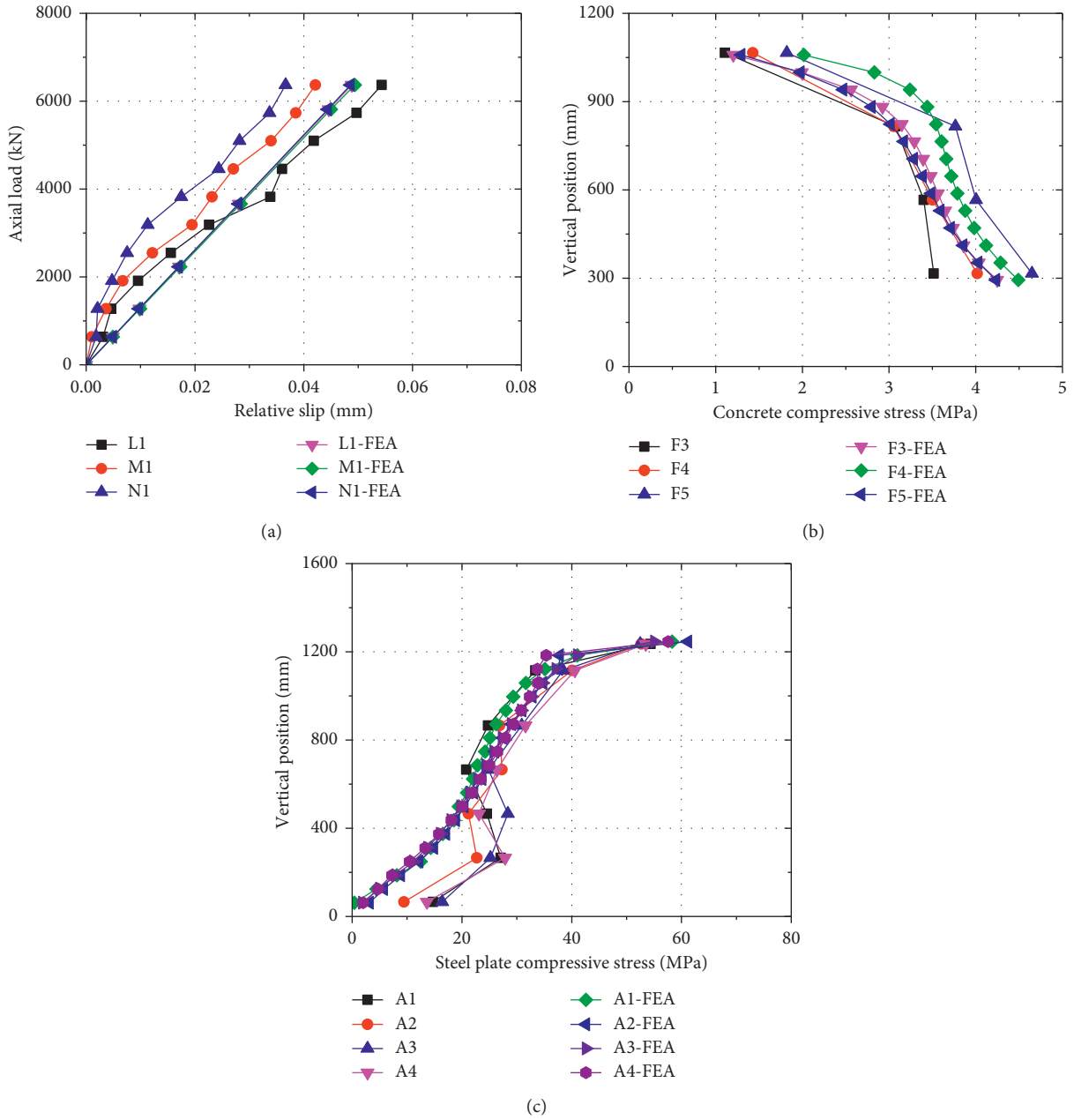

Figure 13: Comparison between FEA and model test results.

axial tensile/compressive stiffness of the concrete component.

6.4. Connector Spacing Effects. Figure 18 shows the axial force sharing ratio distribution between the steel panel and concrete component with the variation of the connector spacing. From the bearing plate downward, the vertical force of the steel structure will gradually reduce to zero and the vertical force of the concrete column will gradually increase to 100%. At the bearing plate, there is an initial sharing proportion between the steel plate wall and the concrete pylon component. The bearing plate transfers the vertical force to the concrete column component through the contact action between the bearing plate and the top surface of the concrete column. With the increase of the connector spacing, the sharing proportion of the initial axial force for the steel structure decreases and the sharing proportion of initial axial force for the concrete column component increases. At the same time, the axial force ratio of the steel wall plate to the concrete column component has an increasing tendency when their location is near the lower end of the joint.

7. Conclusion

(1) Based on the elastic continuous layer method, a theoretical prediction method for the hybrid joint with the

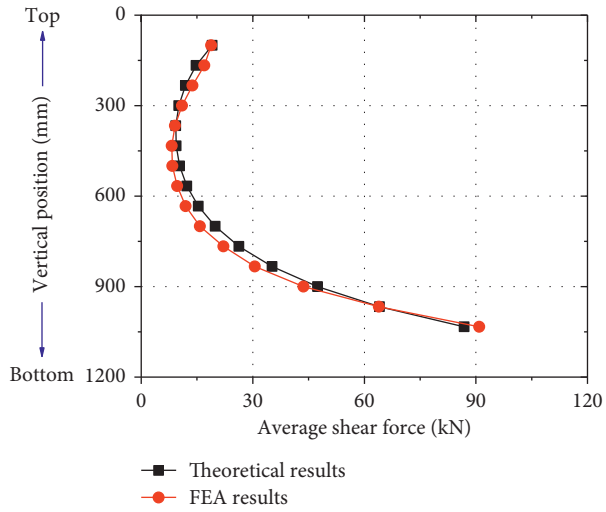

Figure 14: Contrast of shear force distribution.

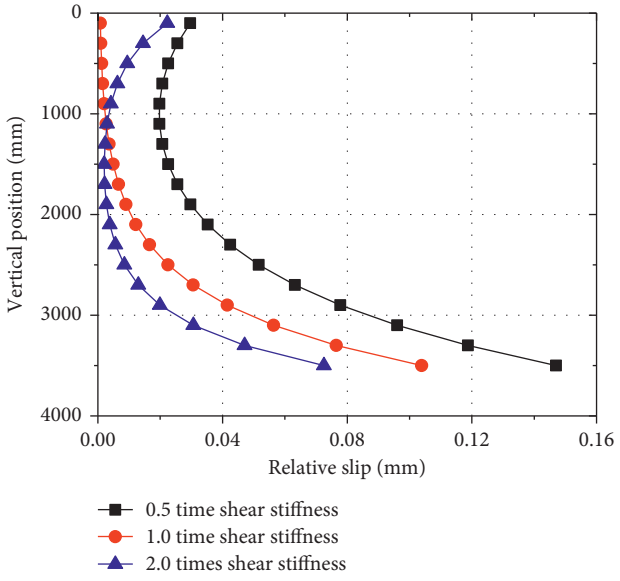

Figure 15: Load-slip curve with various shear stiffness.

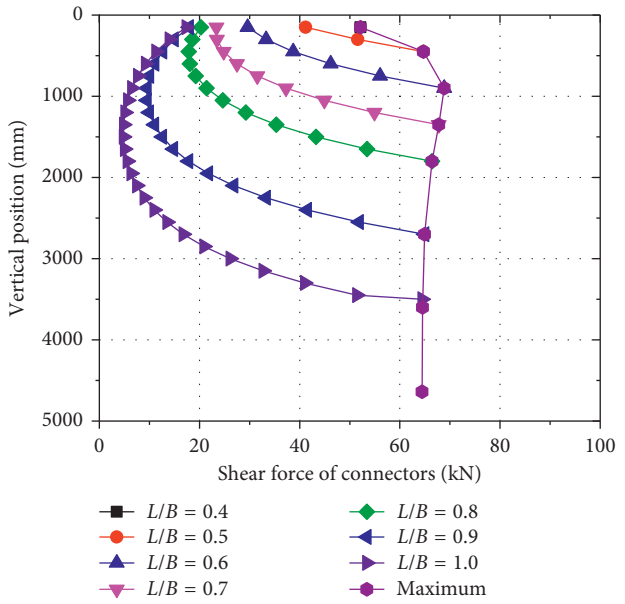

Figure 16: Effect of hybrid joint length on shear force distribution.

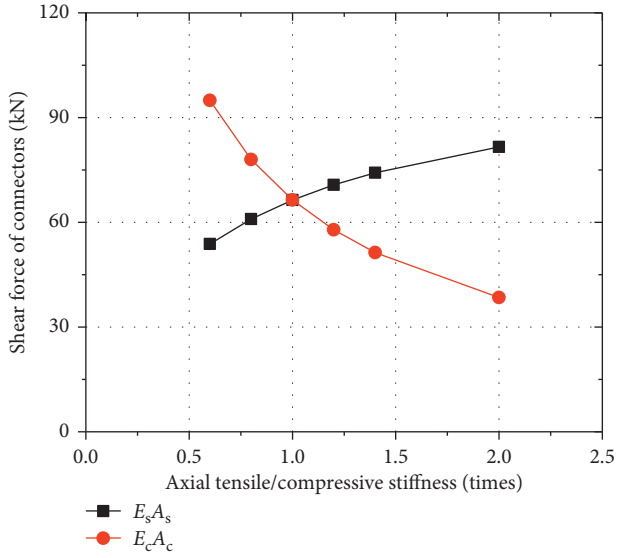

Figure 17: The relationship between the shear force and the axial stiffness of the hybrid joint.

cells and rear bearing plates is given, which could be employed to predict the shear force distribution of the hybrid joint. The slip effect at the steel-concrete interface and the local bearing effect on the internal concrete by the steel bearing plates are both considered in the proposed theoretical model.

(2) A scaled test model for the hybrid joint of the Jishui Gan River Second Bridge was conducted; the stress distribution of the steel and concrete components and the relative slip at the steel-concrete interface were measured and compared with the finite element analysis and the theoretical analysis results. The theoretical analysis results have a good agreement with the model test results, proving the accuracy of the proposed theoretical analysis method.

(3) The proposed theoretical analysis method was employed to explore the load transfer mechanism; it is concluded that, with the increase of the distance from the top bearing plate to the bottom of the hybrid joint, the relative slip will decrease firstly and then increase till the bottom of the hybrid joint. The maximum shear force of the connectors at the steel-concrete interface will have an increasing tendency with the increase of the axial tensile/compressive stiffness of the steel plate. With the increase of the connector spacing, the sharing proportion of the initial axial force for the steel structure decreases, and the sharing proportion of initial axial force for the concrete column component increases.

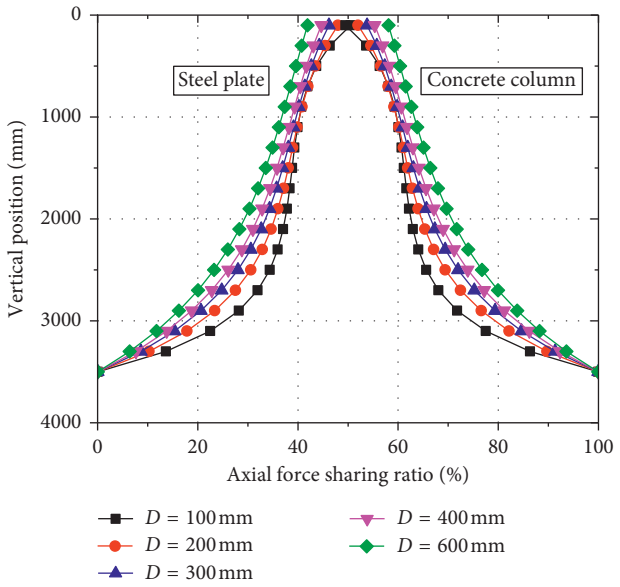

Figure 18: Effect of the connector spacing on the shear force distribution.

Data Availability

The test results of the steel-concrete hybrid joint in this paper are available from the corresponding author upon request.

Conflicts of Interest

The authors declare that they have no conflicts of interest.

Acknowledgments

This work was financially supported by the National Natural Science Foundation (Grant no. 51578406) of People's Republic of China.

References

[1] H. Xin, Y. Liu, J. He, and Y. Zhang, "Experimental and analytical study on stiffened steel segment of hybrid structure," *Journal of Constructional Steel Research*, vol. 100, pp. 237–258, 2014.

[2] J. He, Y. Liu, and B. Pei, "Experimental study of the steel-concrete connection in hybrid cable-stayed bridges," *Journal of Performance of Constructed Facilities*, vol. 28, no. 3, pp. 559–570, 2014.

[3] R. Liu and Y. Liu, "Analysis of auxiliary ribs in steel-concrete joint of hybrid girder," *Journal of Constructional Steel Research*, vol. 112, pp. 363–372, 2015.

[4] Q. Zhang, D. Jia, Y. Bao, Z. Cheng, Y. Bu, and Q. Li, "Analytical study on internal force transfer of perfobond rib shear connector group using a nonlinear spring model," *Journal of Bridge Engineering*, vol. 22, no. 10, article 04017081, 2017.

[5] Q. Zhang, S. Pei, Z. Cheng, Y. Bao, and Q. Li, "Theoretical and experimental studies of the internal force transfer mechanism of perfobond rib shear connector group," *Journal of Bridge Engineering*, vol. 22, no. 2, article 04016112, 2017.

[6] Q. Zhang, D. Jia, Y. Bao, Z. Cheng, L. Xiao, and Y. Bu, "Internal force transfer effect-based fatigue damage evaluation for PBL shear connector groups," *Journal of Constructional Steel Research*, vol. 148, pp. 469–478, 2018.

[7] S. E. Kim and H. T. Nguyen, "Finite element modeling and analysis of a hybrid steel-PSC beam connection," *Engineering Structures*, vol. 32, no. 9, pp. 2557–2569, 2010.

[8] S. E. Kim and H. T. Nguyen, "Evaluation of the connection efficiency of hybrid steel-concrete girder using finite element approach," *International Journal of Mechanical Sciences*, vol. 61, no. 1, pp. 8–23, 2012.

[9] S.-H. Kim, C.-G. Lee, J.-H. Ahn, and J.-H. Won, "Experimental study on joint of spliced steel-PSC hybrid girder, Part I: proposed parallel-perfobond-rib-type joint," *Engineering Structures*, vol. 33, no. 8, pp. 2382–2397, 2011.

[10] S.-H. Kim, C.-G. Lee, S.-J. Kim, and J.-H. Won, "Experimental study on joint of spliced steel-PSC hybrid girder, part II: full-scale test of spliced hybrid I-girder," *Engineering Structures*, vol. 33, no. 9, pp. 2668–2682, 2011.

[11] S. He, Z. Fang, Y. Fang, M. Liu, L. Liu, and A. S. Mosallam, "Experimental study on perfobond strip connector in steel-concrete joints of hybrid bridges," *Journal of Constructional Steel Research*, vol. 118, pp. 169–179, 2016.

[12] X. Cheng, X. Nie, and J. Fan, "Structural performance and strength prediction of steel-to-concrete box girder deck transition zone of hybrid steel-concrete cable-stayed bridges," *Journal of Bridge Engineering*, vol. 21, no. 11, article 04016083, 2016.

[13] L. Xiao, X. Li, and Z. John Ma, "Behavior of perforated shear connectors in steel-concrete composite joints of hybrid bridges," *Journal of Bridge Engineering*, vol. 22, no. 4, article 04016135, 2017.

[14] S. He, Z. Fang, and A. S. Mosallam, "Push-out tests for perfobond strip connectors with UHPC grout in the joints of steel-concrete hybrid bridge girders," *Engineering Structures*, vol. 135, pp. 177–190, 2017.

[15] C. Zhao, Z. Li, K. Deng, and W. Wang, "Experimental investigation on the bearing mechanism of perfobond rib shear connectors," *Engineering Structures*, vol. 159, pp. 172–184, 2018.

[16] S. He, A. S. Mosallam, Z. Fang, C. Zou, W. Feng, and J. Su, "Experimental study on CFSC encased shear connectors in steel-concrete composite joints with UHPC grout," *Construction and Building Materials*, vol. 173, pp. 638–649, 2018.

[17] Z. Li, C. Zhao, K. Deng, and W. Wang, "Load sharing and slip distribution in multiple holes of a perfobond rib shear connector," *Journal of Structural Engineering*, vol. 144, no. 9, article 04018147, 2018.

[18] JTG/T D64-01, *Specifications for Design and Construction of Highway Steel-Concrete Composite Bridge*, China Communication Press Co., Ltd., Beijing, China, 2018.

[19] Z. Lin, Y. Liu, and J. He, "Behavior of stud connectors under combined shear and tension loads," *Engineering Structures*, vol. 81, pp. 362–376, 2014.

[20] Z. Lin, Y. Liu, and C. W. Roeder, "Behavior of stud connections between concrete slabs and steel girders under transverse bending moment," *Engineering Structures*, vol. 117, pp. 130–144, 2016.